Modeling anticancer drug–DNA interactions *via* mixed QM/MM molecular dynamics simulations†

Katrin Spiegel[a] and Alessandra Magistrato*[b]

Received 22nd March 2006
First published as an Advance Article on the web 17th May 2006
DOI: 10.1039/b604263p

The development of anticancer drugs started over four decades ago, with the serendipitous discovery of the antitumor activity of cisplatin and its successful use in the treatment of various cancer types. Despite the efforts made in unraveling the mechanism of the action of cisplatin, as well as in the rational design of new anticancer compounds, in many cases detailed structural and mechanistic information is still lacking.
Many of these drugs exert their anticancer activity by covalently binding to DNA inducing a distortion or simply impeding replication, thus triggering a cellular response, which eventually leads to cell death. A detailed understanding of the structural and electronic properties of drug–DNA complexes and their mechanism of binding is the key step in elucidating the principles of their anticancer activity. At the theoretical level, the description of covalent drug–DNA complexes requires the use of state-of-the-art computer simulation techniques such as hybrid quantum/classical molecular dynamics simulations.
In this review we provide a general overview on: drugs which covalently bind to DNA duplexes, the basic concepts of quantum mechanics/molecular mechanics (QM/MM), molecular dynamics methods and a list of selected applications of these simulations to the study of drug–DNA adducts. Finally, the potential and the limitations of this approach to the study of such systems are critically evaluated.

[a]*University of Pennsylvania, Department of Chemistry, Philadelphia, PA, USA*
[b]*CNR-INFM-Democritos National Simulation Center and International School for Advanced Studies (SISSA/ISAS), Trieste, Italy*
† Electronic supplementary information (ESI) available: Mechanism of binding of the azole-bridged diplatinum drugs to guanine bases (Fig. S1), and dihedral angles around the amide link (Table S1). See DOI: 10.1039/b604263p

1 Introduction

The successful development of metal-containing anticancer agents began with *cis*-[$PtCl_2(NH_3)_2$] (**1**, Fig. 1) often referred to as cisplatin,[1] the anticancer activity of which was fortuitously discovered by Rosenberg *et al.* in 1964.[2] Currently, cisplatin is the most widely used anticancer drug with particular efficiency in

Katrin Spiegel was born in 1975 in Aarau, where she spent her high-school years. After two years of undergraduate classes in chemistry at the Université de Lausanne and the Ecole Polytechnique de Lausanne, she moved to the ETH at Zurich and received her graduate degree in spring 2000, working with Prof. U. Rothlisberger. She then moved to Italy, to the International School of Advanced Studies (SISSA, Trieste), where she received her PhD in biological and statistical physics with Prof. P. Carloni in 2004. Currently, she is a postdoc at the University of Pennsylvania, where she is working in the group of Prof. M. L. Klein, focusing on the description of drug–DNA systems and the improvement of de novo *designed proteins.*

Katrin Spiegel

Alessandra Magistrato

Alessandra Magistrato was born in Orvieto, Italy, in 1973 where she attended high school. In 1997 she received her graduate degree in Chemistry at the University of Perugia, Italy. She moved then to Switzerland where she obtained her PhD in Computational Inorganic Chemistry in 2001 at ETH Zentrum, Zurich, working in the group of Prof. U. Rothlisberger. From 2001 to 2003 she was a postdoctoral fellow at the University Of Pennsylvania, Philadelphia, USA in the group of Prof. M.L. Klein. Since 2003 she has been Assistant Professor of Theoretical and Computational Biophysics at the CNR-INFM-Democritos National Simulation Center and at the International School for Advanced Studies (SISSA/ISAS), Trieste, Italy. Her research interests are devoted to the computational study of the mechansim of action of antitumor drugs and to the study of pharmacologically relevant metallo-enzymes.

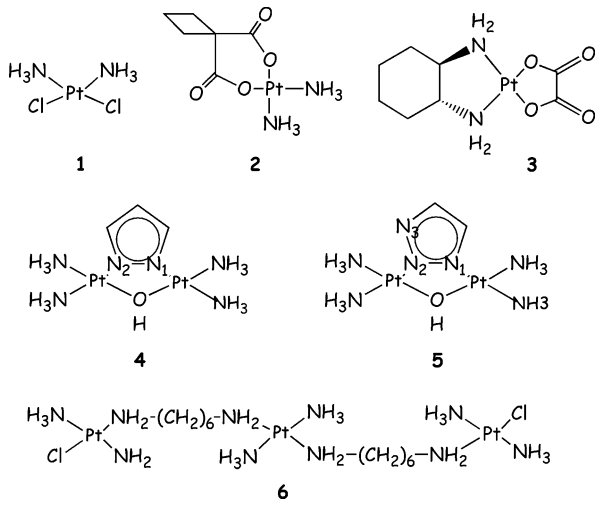

Fig. 1 Structure of cisplatin (**1**), carboplatin (**2**), oxaliplatin (**3**), dinuclear ([*cis*-{$Pt(NH_3)_2$}$_2$(μ-OH)(μ-pz)]$^{2+}$(**4**) and [*cis*-{$Pt(NH_3)_2$}$_2$-(μ-OH)(μ-1,2,3-tz)]$^{2+}$ (**5**)) and trinuclear platinum antitumor drugs (**6**).

testicular, ovarian, head and neck cancers (where cure rates up to 90% are commonly obtained).[1–4]

The major drawbacks in the use of cisplatin reside in its intrinsic and acquired resistance, which limits its application to sensitive cancer cells. Furthermore, when administered to patients, cisplatin causes severe side effects, such as nausea, ear damage and vomiting.[1] These limitations have prompted the design of new anticancer drugs, starting from simple cisplatin derivatives (second generation), to more complex dinuclear- or trinuclear species (third generation), to drugs containing transition metals other than platinum. Unfortunately, second generation Pt-drugs, such as carboplatin and oxaliplatin (**2**, **3**, Fig. 1), also suffer from drug resistance and side effects.[1,2,5–7] Third generation Pt-drugs with different oxidation states are commonly believed to be prodrugs of classical cisplatin agents, rather then new drugs.[8,9] In contrast, dinuclear and trinuclear Pt complexes (**5–7**, Fig. 1) represent a promising alternative to cisplatin, since they have been especially designed to cause a different cellular response than cisplatin, reducing the risk of both cross- and intrinsic resistance.[1,8]

Among many other transition metal compounds tested, only ruthenium complexes have attracted interest as potential anti-cancer agents,[1,10,11] demonstrating a cytotoxic activity different from that of cisplatin. In contrast to Pt-drugs, the cellular target of ruthenium complexes has not been unambiguously identified,[10,11] and a detailed understanding of their mechanism of action is a highly challenging task.

A completely different cytotoxic activity is expected from antitumor antibiotics (Fig. 2). These drugs contain several aromatic heterocycles, and they exert their anticancer activity by covalently binding to the minor groove of DNA with high sequence specificity.[12,13] Among them, anthramycin (**8**) and duocarmycins (**9–11**) (Fig. 2) are exceptionally potent antitumor antibiotics whose derivatives have recently entered clinical trials.[14,15] Although many hypotheses have been formulated about the origin of their sequence selectivity and a potential catalytic role of DNA in their binding, these issues are far from completely elucidated. A detailed understanding of the factors that govern minor groove binding and reactivity is clearly of great pharmacological interest, as it may provide the basis for the design of more active anticancer agents.

Nowadays, theoretical calculations of molecular and electronic structure represent a valuable complement to experiments to elucidate structure–activity relationships and to study the mechanism of drug binding at the molecular level. Over the last few years many theoretical studies have been performed on cisplatin as a prototype of metal-containing anticancer drugs. These studies are

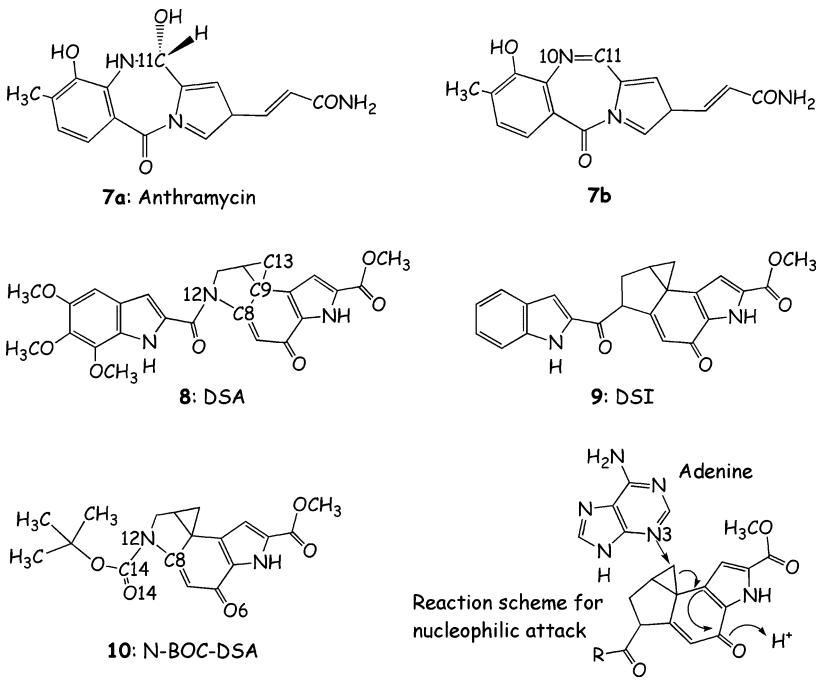

Fig. 2 Anthramycin (**7a**) and anhydroanthramycin (**7b**), **DSA** (**8**) and **DSI** (**9**) and **NBOC-DSA** (**10**) duocarmycin derivatives. Schematic drawing of nucleophilic attack of adenine to **NBOC-DSA**.

mainly based either on traditional quantum mechanical electronic structure calculations of small models of the drug[16–21] and drug–nucleoside complexes,[22–26] or classical molecular dynamics simulations of the cisplatin–DNA adducts.[27,28] In addition, due to the increasing pharmacological potential of ruthenium-containing drugs[10] and aromatic antibiotics,[14,15] quantum mechanical studies have recently appeared that try to identify their binding[29] and reaction mechanism.[30,31]

However, both classical molecular dynamics (MD) and quantum mechanical (QM) studies of a drug covalently linked to DNA present severe drawbacks. Classical MD studies based on predefined force fields might encounter difficulties in describing anticancer metal-containing drugs, since their structural and energetic properties depend in an intricate way on the electronic structure of the transition metal ion,[32,33] while purely organic drugs bonded to DNA invariably contain non-standard groups, for which an accurate classical parametrization is usually not available. QM calculations overcome these problems by explicitly taking into account the electronic structure of the drug, thus elegantly avoiding the parametrization of force fields for uncommon organic or inorganic (metal-containing) molecules. In addition, in the framework of an *ab initio* molecular dynamics scheme, they allow the direct simulation of bond forming and bond breaking in biochemical reactions.[32,33] However, QM methods are computationally quite expensive and their treatment is usually restricted to relatively small systems in the gas phase.

Complex biochemical processes occur in a heterogeneous condensed phase environment that comprises several thousands of atoms, and thus a mixed quantum/classical (QM/MM) approach that takes into account accurately the chemically relevant region of the system, while treating the rest of the biomolecular environment at a computationally efficient level, has emerged as a powerful computational tool.[34–37]

In this review, we focus our attention only on certain selected antineoplastic agents such as cisplatin and its derivatives along with antitumor antibiotics, summarizing our recent studies of the structural, electronic and chemical properties of these drug–DNA adducts by QM/MM MD simulations.[38–41]

2 The QM/MM method

The QM/MM approach combines computational methods of different accuracy and efficiency, resulting in an extremely powerful tool for the study of biological systems.[34–37] The partitioning of the systems into two different regions allows concentration of the computational efforts (QM calculations) to the chemically interesting region, while the rest of the system is treated in a computationally efficient manner (MM calculation). For a drug–DNA complex, the quantum chemical region would naturally be the drug and the covalently linked nucleobase(s), while the mechanical and the electrostatic influence of the remaining oligonucleotide and the solvent are treated with empirical force fields (Fig. 3).

The general form of a mixed QM/MM Hamiltonian was introduced by Warshel:[42]

$$\mathcal{H} = \mathcal{H}_{QM} + \mathcal{H}_{MM} + \mathcal{H}_{QM/MM}$$

where $\mathcal{H}_{QM}$ is the *ab initio* Hamiltonian (which can be based on different quantum mechanical approaches, *i.e.* Hartree–Fock, density functional theory (DFT), or semiempirical methods), $\mathcal{H}_{MM}$ is the classical Hamiltonian, which is described by standard biomolecular force fields and comprises bonded interactions (harmonic bonds, angles and dihedrals) and non-bonded interactions (electrostatic point charges and van der Waals interactions).[34,36]

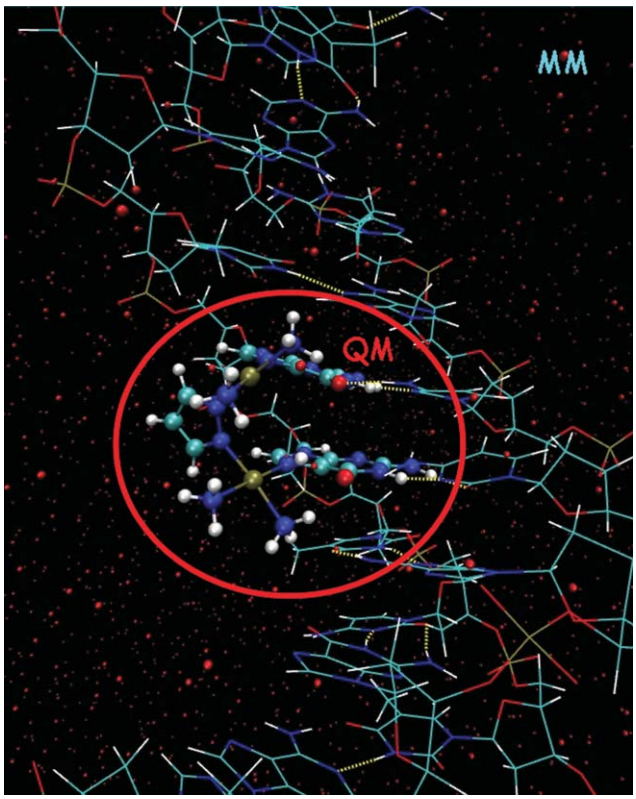

Fig. 3 Example of QM/MM scheme: the metal-containing drug belongs to the QM region (in balls and sticks), the rest of the DNA and the solvent (only oxygen atoms are shown for clarity) (in lines) belong to the MM region.

Invariably, the pitfalls of QM/MM methods lie in the challenge of finding a rigorous treatment of the coupling between the QM and the MM regions as described by the interaction Hamiltonian $H_{QM/MM}$.[34,36]

Several methods have been developed to treat systems where covalent bonds are split between the QM and the MM regions. In the simplest case, either link atoms are used to saturate the dangling bond of the terminal QM atom, or a specially parameterized pseudo-atom is introduced, which mimics closely the modeled group.[34,36] An alternative approach consists in constraining the SCF solution to reflect the influence of the bonds that have been omitted.[34,36] Both approaches have their strengths and weaknesses, but they both lead to good accuracy if treated with appropriate care.[34,36]

The remaining bonding and van der Waals interactions at the interface region are treated classically. Most problematic is the description of the electrostatic interactions between the quantum mechanical and molecular mechanical region.[34,36] The easiest way to electrostatically couple the two regions is a mechanical embedding in which the electrostatic interactions between the QM and the MM parts are either not treated or are treated at the MM level. In an electrostatic embedding the electrostatic effects of

the classical environment are taken into account in the classical description as an additional contribution to the quantum field of the system.[34,36] In this scheme the polarization of the QM region by the MM charge distribution occurs as part of the QM electronic structure calculation.[34,36]

2.1 The hybrid QM (Car–Parrinello)/MM method

The method we have chosen to for the study of anticancer drug–DNA interactions is a combination of *ab initio* (Car–Parrinello) MD,[43,44] and classical MD simulations.

Several mixed QM (Car–Parrinello)/MM schemes have been developed to treat the boundary region between the QM and the MM part.[45–47] In this article we describe applications of the fully Hamiltonian coupling scheme developed by Roethlisberger and co-workers.[46] In this approach, the bonds between the QM and the MM part are treated by the use of monovalent pseudopotentials or by the addition of capping hydrogen atoms. The remaining bonded and van der Waals interactions are treated at the level of the classical force field.

The electrostatic effects of the classical environment are taken into account as an additional contribution to the external field acting on the quantum system, with the addition of a potential function around the location of the classical atoms. This mimics Pauli repulsion with these nuclei, avoiding overpolarization of the electron density near positively charged classical point charges (the electronic spill-out effect).[46] To limit the computational overhead, the electrostatic interactions between the QM system and the more distant MM atoms are included by means of a Hamiltonian term that explicitly couples the multiple moments of the quantum charge distribution with classical point charges.[46]

The Car–Parrinello code CPMD (based on DFT)[48] is interfaced with the classical force field parm99[49,50] in combination with particle mesh Ewald summations to treat long-range electrostatic interactions.[51] This code has been successfully applied to the study of the structural and electronic properties, and the chemical reactivity of complex biological systems containing 10 000–100 000 atoms.[52]

3 Covalent anticancer drug–DNA binding

3.1 Platinum anticancer drugs

Cisplatin. Due to its wide range of applicability in cancer treatment, cisplatin is widely studied both experimentally[1–9] and theoretically.[16–28] Solvolysis, alkylation reaction rates and the structural consequences of cisplatin binding to DNA are well understood and documented.[1–9] It is well known that cisplatin binds to two adjacent guanines, forming preferentially N7(G)–N7(G) intrastrand crosslinks, and that the formation of cisplatin–DNA adducts induces a large kink towards the major groove, a local unwinding at the platinated lesion and a flattening of the minor groove. The shallow minor groove and the large axis bend formed after the binding of cisplatin are recognized by a series of proteins, which bind to the distorted cisplatin–DNA adduct with high affinity. This binding inhibits the replication and transcription machinery of the cell, leading eventually to cell death.[1–7]

The wealth of available structural data makes the cisplatin–DNA adduct a perfect candidate to benchmark the accuracy and the predictability of the QM/MM method in the description of drug–DNA interactions. To this end, we carried out three simulations, starting from the X-ray structures of platinated DNA (**A**)[53] and the cisplatin–DNA adduct in complex with high mobility group (HMG) protein (**B**),[54] as well as from cisplatin docked to the same oligomer (of **A**) in canonical B-DNA conformation (**C**).[38,55,56]

Both **A** and **B** reproduce the relevant experimental structural features with good accuracy (see Table 1). Interestingly, **A** slightly rearranges during the dynamics and adopts a large kink and roll angle, similar to the characteristics of the NMR solution structure (Table 1).[57] In contrast, in **B**, no significant rearrangements occur with respect to the crystal structure. In fact, the HMG protein stabilizes and increases the kink of double strand (ds) DNA induced by the binding of cisplatin.[54,58] In agreement with experiments, Watson–Crick hydrogen bonds are maintained almost entirely,[38] even though the DNA duplex is very flexible in all three simulations. The simulated cisplatin–DNA adducts are shown in Fig. 4.

Surprisingly in **C**, even within the limited time scale of a few picoseconds (7 ps), the DNA undergoes remarkable structural changes, namely a large increase in the kink along with an increase of the roll angle and the rise (Table 1).[58] During the simulation, the helical parameters approach asymptotically the values of simulation **A**, but a complete structural agreement of **C** is impeded by the puckering of the sugars. Indeed, conformational changes of the sugar occur on a time scale of hundreds of ps, and thus they are not accessible in our simulation time scale. Nevertheless, the extent to which DNA can rearrange in a few ps suggests that our method may qualitatively predict structural changes of drug–DNA adducts, for which limited structural information is available.

Dinuclear azole-bridged platinum complexes. Azole-bridged dinuclear platinum(II) compounds (**4** and **5**, Fig. 1)[59,60] have been especially designed to bind DNA, inducing minimal distortions.[1] In principle, small structural changes may render the platinated lesion less recognizable by excision repair enzymes, overcoming the problem of cross-resistance.[1,5]

In agreement with this hypothesis, the NMR structure of the **4**–DNA complex (the only available structural information of a diplatinated drug–DNA complex) shows structural parameters very close to that of canonical B-DNA (Table 1).[1,61] Recently, both **4** and **5** have been shown to have an improved cytotoxic behavior relative to cisplatin in several tumor cell lines, and to circumvent the cross-resistance to cisplatin.[62,63]

Experiments show that the mechanism of binding of **5** to dsDNA is quite complex. In fact, after the first alkylation step, nucleophilic attack of the second guanine can occur or, alternatively, Pt2 (and its coordination sphere) can migrate from N2 to N3, followed by the second alkylation step (for a detailed reaction scheme see Fig. S1 in the ESI†). Therefore, **5** can alkylate two adjacent guanines of dsDNA in both an N1,N2 and an N1,N3 fashion. The N1,N3 isomer presents a larger intermetal distance and can lead to the formation of a variety of inter- and intrastrand crosslinks, which may be a key factor for the high cytotoxicity of these drugs.[62,63]

Table 1 Selected helical parameters at the N7(G)–N7(G) crosslink formed by Pt-drugs binding to DNA : a) cisplatin–5′-d(CpCpTpCpTpG*pG*-pTpCpTpCpC)-3′ complexes **A**, **B** and **C** compared to experimental data;[53,54,57] b) [{*cis*-$Pt(NH_3)_2$}$_2$(μ-OH)(μ-pz)]$(NO_3)_2$ (pz = pyrazolate) (**4**) and [{*cis*-$Pt(NH_3)_2$}$_2$(μ-OH)(μ-1,2,3-ta-N1,N2)]$(NO_3)_2$ (ta = 1,2,3-triazolate) (**5**) bound to 5′-d(CpTpCpTpG*pG*pTpCpTpCp)-3′, resulting in complexes **D**, **E** and **F**, compared to NMR structure,[61] and reference simulation of unbound decamer with same sequence (DNA MD). Rise, major and minor groove width (*W*) and depth (*D*) are given in Å. Roll, tilt, twist, local angle and global axis curvature are in degrees.[58] The minor and major groove parameters refer to the largest value measured at the platinated site (G–G step)

a)	**A**		**B**		**C**		X-Ray		X-Ray HMG		NMR	
Rise	4.3 ± 0.5		7.7		5.0		3.5		7.7		5.7	
Roll	42 ± 9		61 ± 7		28 ± 8		29		64		46	
Tilt	−16 ± 7		−27 ± 4		−14		−7		−26		−21	
Twist	34		2		24		25		30		35	
Local angle	18		36		16		18		31		31	
Global axis curvature	51 ± 10		57 ± 5		48 ± 8		40		46		85	
Groove parameters	*W*	*D*	*W*	*D*	*W*	*D*	*W*	*D*	*W*	*D*	*W*	*D*
Minor groove	8.5	2.5	11.4	0.4	8.9	2.9	9.6	1.4	10.3	−0.8	9.8	1.7
Major groove	4.5	10.9	4.3	9.0	15	6	5.5	9.8	5.3	7.9	9.4	12.1

b)	**D**		**E**		**F**		DNA MD		NMR	
Rise	3.6 ± 0.2		3.6 ± 0.2		4.1 ± 0.3		3.4 ± 0.2		3.3	
Roll	9 ± 4		4 ± 4		−5 ± 5		−3 ± 7		5	
Tilt	8 ± 3		8 ± 3		18 ± 4		−4 ± 5		10	
Twist	31		32		35		38		27	
Local angle	7 ± 2		4 ± 1		6 ± 1		4 ± 2		3	
Global axis curvature	19 ± 5		10 ± 3		8 ± 4		19 ± 8		5	
Groove parameters	*W*	*D*	*W*	*D*	*W*	*D*	*W*	*D*	*W*	*D*
Minor groove	6.1	5.0	6.8	5.2	4.6	5.4	7.0	4.7	7.3	5.0
Major groove	14.9	7.4	11.9	4.1	20.9	3.2	12.9	6.1	16.3	7.9

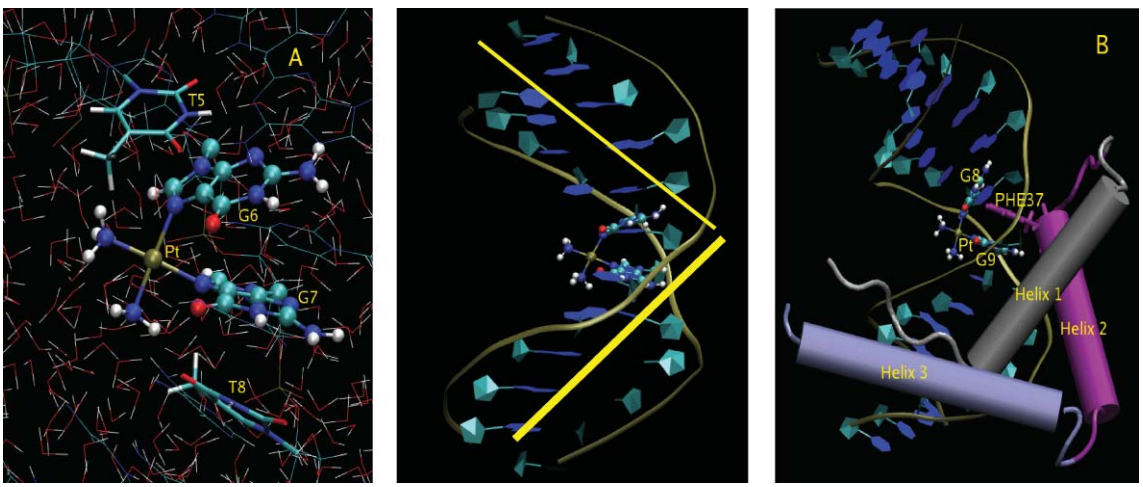

Fig. 4 Left: Close-up QM/MM structure for model **A**, showing quantum region in balls and sticks, adjacent nucleobases as cylinders and the remaining part as lines. Middle: cisplatin–DNA adduct. The kink towards the major groove is shown by yellow lines. Right: Binding of HMG–protein to cisplatin–DNA adduct in **B**. The platinated moiety is shown as ball and sticks, while the intercalating aminoacid PHE37 is shown in sticks (purple).

We have performed an extensive computational study on **4** and **5**, starting from detailed QM calculations in the gas phase of the two drugs, the intermediates and the products of binding to two guanine bases.[39] Our QM calculations suggest that the N2–N3 isomerization of **5** is driven by a large thermodynamic stabilization of the N1,N3 isomer (−20 kcal mol^{-1}) due to the formation of an allylic structure over the three nitrogens of the triazolate unit.[39]

As shown in the previous section, the QM/MM approach has been valuable in characterizing the structural properties of the cisplatin–DNA adduct,[38] and we employed it here to characterize and predict the structural features of **4** and **5** in complex with the dsDNA decamer (**D**–**F**, Fig. 5). The NMR structure of the **4**–DNA complex has been used as a template to construct models of **5**–DNA adducts, considering both the N1,N2 and the N1,N3 binding modes (**E** and **F**, Fig. 5), for which no structural information was available.

The average QM/MM structure of **D** compares well with the NMR structure, thus validating our computational setup. As a general feature, the drug–DNA complexes **D** and **E** display almost the same structural properties, whereas a slightly different structure is observed for **F**, due to its larger intermetal distance.[39]

The following trends are observed (Table 1): (i) A decrease in the roll angle and an increase of the tilt of the platinated G5–G6 bases, when going from **D** to **F**. In **F** a large tilt and negative roll result in a local angle[64] between the G5–G6 base pair step similar to **D** and **E**. However, this angle is smaller in **D**–**F** than in

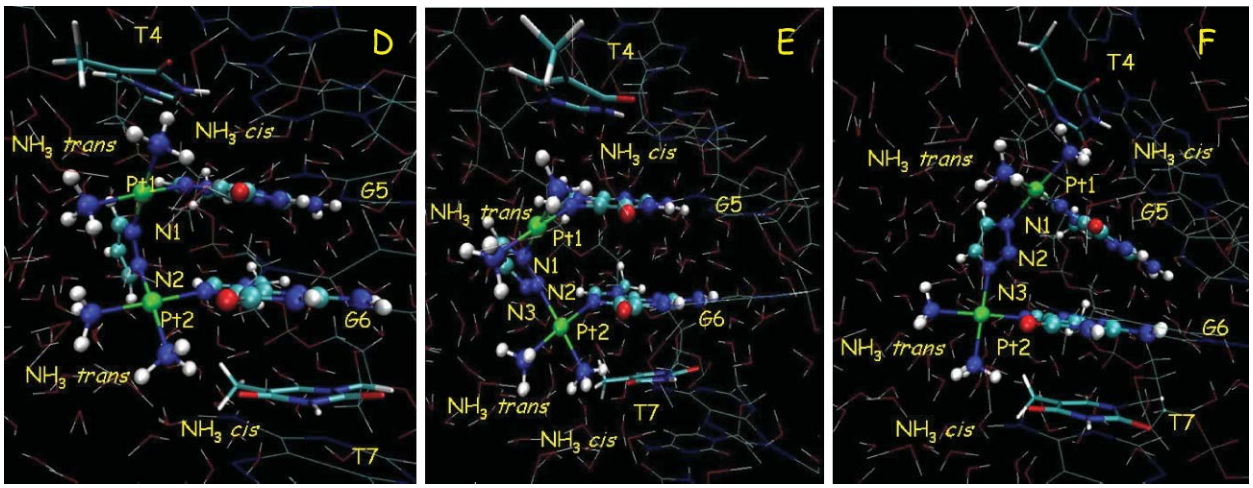

Fig. 5 Average structure for modelx **D**, **E** and **F**. Atoms depicted by balls and sticks belong to the QM region; the remaining atoms and the solvent belong to the MM region. Hydrogen bonds between T4/T7 and the NH_3 *cis*-ligands are depicted by sticks.

cisplatin–DNA;[38] (ii) An increase of the rise at the platinated G5–G6 base step, which in **F** becomes comparable to that observed in cisplatin–DNA adducts;[38] (iii) An increase of the twist from **D** to **F**, which for the latter leads to values typical of canonical B–DNA. This is possibly due to a larger intermetal distance, which increases the flexibility of the diplatinated moiety; (iv) A larger major groove with respect to canonical B–DNA; and (v) a small overall axis bend for all three complexes.[65]

Interestingly, cisplatin has exactly the opposite effect on the helical parameters, giving thus a rationale for the lack of cross-resistance of these drugs.[38,39] In principle, the absence of a pronounced kink and no significant changes in minor groove width may render the platinated lesion less recognizable to the excision repair enzymes, working around the problem of cellular resistance.[1,5]

Our results, based on QM/MM MD, provide a detailed picture of local distortions at the platinated site, and give some qualitative trends for the global distortions in DNA, such as a decrease in axis curvature observed when going from **D** to **F**.[39,64] Simulations on a longer time scale are, however, required to confirm this trend in global DNA parameters, which reach their equilibrium values much more slowly than local parameters. To this end, accurate force field parameters for the diplatinum moiety (embedded in its biomolecular environment) have been derived 'on the fly' from the QM/MM trajectories.[66] Classical MD simulations, performed with these parameters, confirm a decrease of the overall axis curvature when going from **D** to **F**, although this is less pronounced.[67]

Here, QM/MM MD simulations have been used as a unique computational tool to predict structural properties of novel diplatinum drug–DNA adducts. Our findings complement the existing experimental data that is available on the mechanism of action of platinum anticancer agents (currently still under debate), and may be crucial for the development of more specific anticancer complexes.

3.2 Antitumor antibiotics

The discovery of the antitumor activity of natural antibiotics has raised a lot of interest.[12,13] These antibiotics are typically extended aromatic systems, which either intercalate between two base pairs, or enter into the minor groove of duplex DNA with high sequence selectivity.[12,13] Some of them form covalent bonds to DNA bases, and here we will focus on this class of antibiotics. Due to the tight binding to the minor groove, the electronic structure of these drugs may be highly perturbed by the electric field of DNA. Thus, a QM/MM approach can be very useful to obtain information about the effect of the biomolecular environment on both the electronic properties and the reactivity of the drugs.

Anthramycin. Anthramycin is a natural antibiotic belonging to the family of pyrrolo-benzodiazepines.[68] Although cardiotoxic, anthramycin is often used as a template in drug design, and recently a number of its derivatives with improved antitumor activity have entered into clinical trials.[14] These compounds exert their anticancer activity by binding to the minor groove of dsDNA and by forming subsequently a covalent bond to a guanine. The formation of the covalent complex induces a cascade of cellular events, which eventually lead to apoptosis.[68]

Anthramycin is a prototypical drug for the study of covalent minor groove binders due to the available structural data for the drug–DNA complex[68] and due to its role as a lead in drug design.[13,14]

Currently, the potential catalytic role of the dsDNA on the formation of the covalent bond and the detailed mechanism of binding are not completely elucidated. In addition, there is still an ongoing debate concerning whether the hydroxy (**ant**, **7a** in Fig. 2) or anhydrido (**imi**, **7b** in Fig. 2) form of the drug is the reactive species, which undergoes the nucleophilic attack by N2(Gua).[69]

Hybrid QM/MM simulations of the two non covalent (**imi**/DNA and **ant**/DNA) adducts have been performed to investigate the catalytic role of DNA in the alkylation step, as well as attempting to shed light on the relative reactivity of the two complexes.[40] The QM/MM scheme has been adopted to split the source of polarization into various contributions: either including the electrostatic effects of DNA and solvent (*with bioframe*) or switching it off (*without bioframe*).[40]

A comparison of the electrostatic potential with and without the biomolecular environment shows that the explicit electrostatic effect of DNA induces significant differences between the reactive

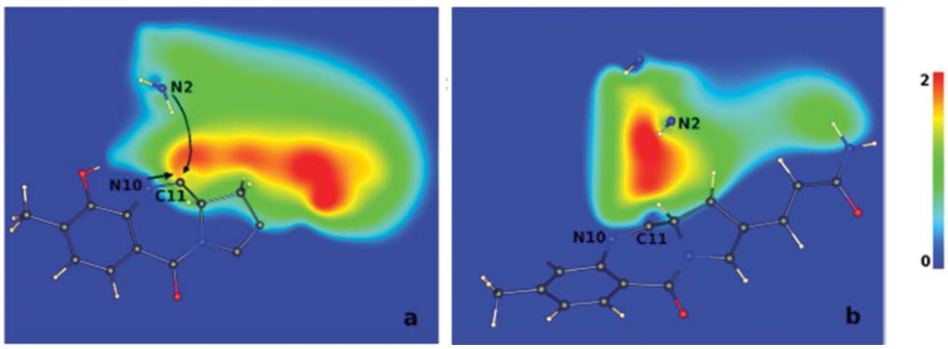

Fig. 6 Contour plots of the difference in the electrostatic potential (eV) with or without the biomolecular frame (calculated within the QM region through the plane defined by N2, N10, C11) for (a) anhydro-anthramycin and (b) hydroxy-anthramycin.

centers (N2@Gua and C11@drug, Fig. 6). In **imi**/DNA the alkylation reaction may be promoted by a gradient of the electrostatic potential. This gradient renders C11@drug (which undergoes the nucleophilic attack of N2@Gua) more electrophilic, and it may assist the alkylation process. In contrast, in **ant**/DNA the largest effect is in proximity of N10@Gua, and no gradient is present between the reactive centers.

The effect of the polarization of both the drug and the dsDNA is also monitored by calculating the bond ionicities (BI)[70] of reactive bonds and the energy gap between reactive orbitals. In these calculations we have separately monitored the effect of the DNA and the solvent.

The most pronounced polarization effects occur for the lone pair of N2@Gua of **ant**, and for the N10–C11@drug π-bond of **imi** (Table 2). These are mainly due to the electrostatic field of the DNA, while the effect of the water molecules is negligible. Finally, the gap between reactive orbitals (involved in bond formation and breaking), is significantly decreased in the presence of the DNA environment, suggesting that the drug is activated when it resides in the minor groove of dsDNA.

Therefore, these results reveal unambiguously that the dsDNA-environment can assist the alkylation process by altering the electrostatic potential between the reactants. In addition, this qualitative analysis suggests that **imi** may be more reactive than **ant**, but it does not allow discrimination of the two forms with certainty. A clear indication of the relative reactivity of the two drugs requires calculations of the activation free energy barrier for the reaction of binding to DNA, an example of which is given in the next section.

Duocarmicyns. We studied the detailed binding mechanism of three duocarmycin derivatives (Fig. 2), namely (+)-duocarmycin SA (**DSA**), (+)-duocarmycin SI (**DSI**), and **NBOC-DSA** (**8–10**, respectively). The cytotoxic potential of these drugs arises from their binding to the DNA minor groove and from the subsequent alkylation at the N3@Ade site.[71–75] Alkylation occurs by an S_N2 reaction, in which the cyclopropyl ring is opened by nucleophilic attack of N3@Ade at the least-substituted carbon atom of the drug (C13@drug in Fig. 2). The relative reactivity of duocarmycins towards DNA decreases in the order **DSA** > **DSI** ≫ **NBOC-DSA**.[75] Interestingly, these drugs are stable in water, and undergo solvolysis only at pH 3.

Clearly, the DNA environment has a fundamental role in the reactivity of duocarmycins. Several hypotheses have been made regarding the effects of the DNA in activating the alkylation of the duocarmycins: (i) a conformational change in DNA upon drug-binding may render the adenine base more reactive;[76] (ii) The drug, when bound to DNA, experiences a conformational change around the amide link. The distortions around the amide bonds could reduce the π-electron conjugation and ultimately destabilize the cyclopropyl unit[75,77,78] (shape-induced activation); and (iii) general- or specific acid catalysis or cation complexation

Table 2 (a) Bond ionicities of N2@G and N10–C11@drug bonds. *With bioframe*, *Without bioframe* and *Without solvent* refer to the calculation with both DNA and solvent, without both DNA and solvent, and with DNA and without the solvent, respectively. The last column refers to the calculation *in vacuo*. (b) HOMO–LUMO gap between the Kohn–Sham energy levels that correspond to orbitals localized on the reactive centers

a)		With bioframe	Without bioframe	Without solvent	*In vacuo*
Imi/DNA	C11–N10	0.57, 0.58 ± 0.01	0.54, 0.55 ± 0.01	0.58, 0.59 ± 0.01	0.55, 0.56
	N2 lone pair	0.21 ± 0.05	0.19 ± 0.05	0.21 ± 0.07	0.24
Ant/DNA	C11–N10	0.57 ± 0.01	0.57 ± 0.01	0.58 ± 0.01	0.57
	N2 lone pair	0.20 ± 0.05	0.15 ± 0.06	0.15 ± 0.06	0.24

b)	Energy gap/eV	
	Imi/DNA	**Ant**/DNA
With bioframe	Δ(LUMO/HOMO-2) ~ 1.4	Δ(LUMO/HOMO) ~ 1.2
Without solvent	Δ(LUMO/HOMO-1) ~ 1.3	Δ(LUMO + 1/HOMO) ~ 2.1
Without bioframe	Δ(LUMO/HOMO-1) ~ 1.9	Δ(LUMO + 1/HOMO) ~ 3.2

to the O6 group could increase the electrophilicity of the cyclopropyl unit.[79,80]

Recent *ab initio* studies have investigated the reaction mechanism of several duocarmycin derivatives, but they did not include the DNA environment.[30,31] Since the DNA has been postulated to play a fundamental catalytic role, we have addressed this issue by studying the structural and electronic properties of **8–10** and the reaction energy profile of the nucleophilic attack of N3@Ade upon C13@drug of **8–10** in their explicit biomolecular environment.[41]

An analysis of the structural properties of reactant and transition state structures shows no significant discrepancies in the torsional angle profile of the three drugs (Table S1†) or in the bond orders around the amide link (Table 3), suggesting that the shape-induced mechansim plays a minor role.

The free energy profile for the alkylation step of **8–10** has been obtained by thermodynamic integration, choosing as a reaction coordinate the distance between N3@Ade and C13@drug.[81] A qualitative measure of the catalytic effect of DNA is obtained by comparing the activation free energy calculated for the alkylation process of **10** in water or in the minor groove of dsDNA.

The reaction energy profile for the covalent binding to DNA is fairly similar for the three drugs (Table 3). The small differences may be attributed to the slightly different positions that the drugs assume in the minor groove in the initial classical MD simulations,[55] where the extended aromatic ring system of **8** and **9** allows them to occupy a more favorable position for nucleophilic attack.[41]

On the other hand, a comparison between the alkylation reaction of **10** in water and in dsDNA shows that in the latter the free energy barrier is reduced by 4 kcal mol^{-1}, which corresponds to a rate enhancement of roughly three orders of magnitude. To understand the origin of this rate acceleration, the evolution of the electronic structure along the selected reaction path has been followed in terms of bond ionicities[70] and bond orders (Table 3) for the C9–C13 and the N3–C13 bonds involved in the reaction (Fig. 7).

In general, an early transition state, in which the forming bond is poorly developed and the breaking bond is still quite strong, has a lower activation free energy than a late transition state, in which bond formation and breaking is more advanced. In agreement with this statement, our simulations show that in water, bond breaking and forming has proceeded further than in DNA. Furthermore, BIs indicate that the C9–C13 bond is less polarized in water than in DNA, suggesting that the polarization effects of the DNA render the cyclopropyl unit more reactive (Table 3). Thus, the polarization of the biomolecular frame appears to be a crucial ingredient for the binding of antitumor antibiotics to the minor groove of dsDNA.

4 Concluding remarks and future perspectives

Many important anticancer drugs exert their biological function by covalently binding to DNA.[1,12,13] Experiments yield information about drug binding affinities, reaction rates, cytotoxicity as well as structural information regarding binding to their biological targets. We have reported here a few selected examples in which we show how QM/MM MD simulations can complement these experimental data, to help us to understand better the principles and the mechanism of binding of anticancer drugs at the molecular level.

Table 3 a) Bond orders and bond ionicities[70] for the reactive bonds. In case of BIs we show the values shortly before the TS, because at the TS, the N9–C13 Boys orbital is essentially localized at N9 and can no longer be considered as belonging to N9–C13. Data are shown for the three drug–DNA adducts and for **NBOC-DSA**–adenine in water. b) Activation free energies of the alkylation step of **8–10**

a)		**DSA**–DNA		**DSI**–DNA		**NBOC-DSA**–DNA		**NBOC-DSA**–Ade (water)	
$D_{N3\text{-}C13}$/Å		3.0	2.3	3.0	2.3	3.0	2.3	3.0	2.3
Bond orders	N3–C13	0.008	0.221	0.019	0.208	0.009	0.221	0.009	0.327
	C9–C13	0.809	0.410	0.803	0.411	0.814	0.395	0.815	0.240
	C14–O14	1.504	1.454	1.571	1.512	1.588	1.516	1.572	1.513
	C14–N12	1.104	1.173	1.078	1.130	1.003	1.107	1.022	1.121
	N12–C8	1.096	1.050	1.144	1.076	1.131	1.068	1.120	1.064
$D_{N3\text{-}C13}$/Å		3.0	2.4	3.0	2.4	3.0	2.4	3.0	2.4
Bond ionicities	N3 lone pair	0.374	0.441	0.370	0.424	0.364	0.429	0.392	0.414
	C9–C13	0.379	0.244	0.404	0.262	0.405	0.233	0.415	0.253

b)	**DSA**–DNA	**DSI**–DNA	**NBOC-DSA**–DNA	**NBOC-DSA**–Ade
$\Delta G^{\#}$ (theor.)/kcal mol^{-1}	10.5 ± 3.4	13.8 ± 3.6	12.1 ± 2.4	16.1 ± 4.0
$\Delta G^{\#}$ (exp.)/kcal mol^{-1}	22.7	24.5	26.8–28.2	—

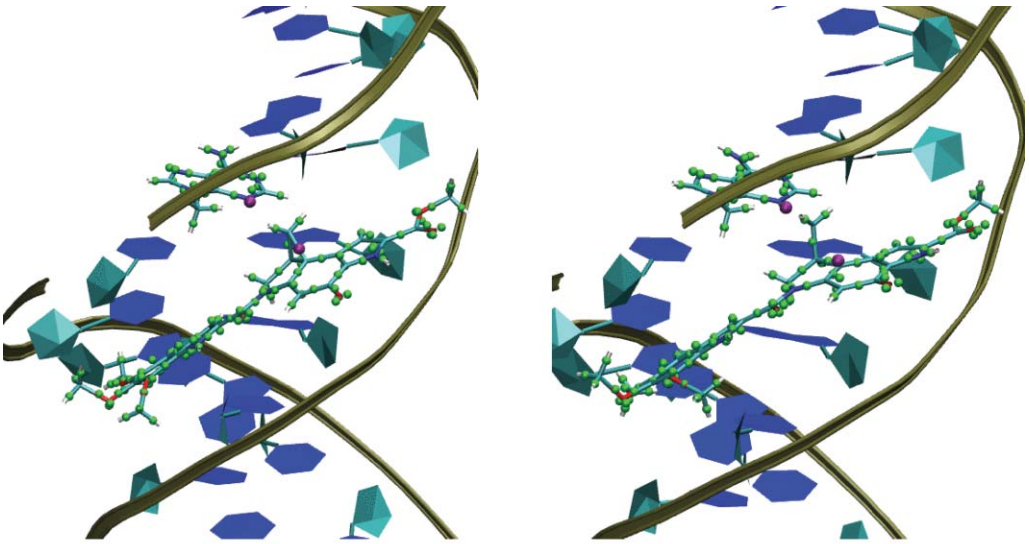

Fig. 7 The electronic structure of **DSA** investigated in terms of localized Boys orbital centers (a) at the ground state, and (b) at the transition state of the alkylation step. Boys orbital centers (shown as green spheres) at the resting state and the transition state provide a visual means of inspecting of the electron density evolution along the reaction path. The Boys orbital centers in N3@Ade and of the C9–C13@drug are highlighted in purple.

Specifically, we have characterized global and local DNA parameters of cisplatin and novel diplatinum drugs in covalent complexes with dsDNA.[38,39] Our simulations show modest structural distortions of the azole-bridged diplatinum–DNA adduct, compared with the large kink in dsDNA induced by cisplatin. These different structural properties may induce diverse cellular responses, accounting for the cytotoxicity of dinuclear drugs in cell lines resistant to cisplatin.[1,5]

A detailed understanding of how these structural differences in cisplatin–DNA and diplatin–DNA adducts may affect protein recognition and other cellular processes triggered by the modified DNA is a highly challenging task. Even though this problem lies outside the possibility of an accurate theoretical study, our simulations do provide hints and additional viewpoints to help interpret experimental findings.

In addition, QM/MM simulations have proved to be a unique tool to give a qualitative picture of the catalytic effect of DNA in the binding of antitumor antibiotics.[40,41] The possibility to switch the DNA environment on or off helps in elucidating the effect of the biomolecular frame on the electronic structure[40] and on the reactivity of the drugs.[41] Our simulations have shown that rate enhancement is achieved primarily through polarization of the reactants.[40,41] A detailed knowledge of these properties, along with the reaction mechanism, may guide experimenters towards the design of more active drugs.

We have also shown that activation free energy barriers and reaction mechanisms can be studied within the QM/MM scheme, monitoring the changes of the electronic structure 'on the fly' (along the reaction path).

One of the major drawbacks of hybrid QM/MM MD simulations is the limited time scale (a few tens of picoseconds),which clearly limits the accessibility of many relevant biological events. The use of enhanced sampling techniques[82–85] allows improving the accessibility of the entire phase space and observing rare events.

Among these computational techniques, the QM/MM metadynamics scheme[85] appears to be a promising computational tool to predict reaction mechanisms of complex chemical and biochemical processes without the bias of few arbitrarily selected reaction coordinates.[86]

Another useful application of QM/MM MD is the derivation of accurate force field parameters at no additional computational cost.[65] Empirical parameters for new metal-containing anticancer compounds or molecules, which are difficult to access by experiment, such as reaction intermediates, can appropriately be derived, with the advantage of implicitly taking into account the biological framework and temperature effects.[65] In this framework, a combination of classical MD and QM/MM MD allows great extension of the potential of molecular simulations in the study of anticancer drugs and their interactions with biological targets.[66]

From the genetic point of view, cancer is a multifactorial disease dependent on the simultaneous deregulation of more than one gene. The genes involved in the onset of the disease are the same that regulate "normal" functions in healthy cells, and therefore they are not specific and selective targets for the control of the disease. However, in the post-genomic era, cancer research has focused on the transduction of signaling pathways characteristic of tumor cells, and it is likely that in the future attention will be devoted towards targets other than DNA. To this end, the use of state-of-the-art computer simulations will be valuable to help support the study of the interactions of anticancer drugs with these newly identified targets.

Acknowledgements

The authors thank Prof. P. Carloni who suggested some of these studies and, along with Prof. P Ruggerone and A.V. Vargiu, contributed to this work. We also thank Prof. U. Röthlisberger and Prof. M. L. Klein for their support and Dr. R. Rousseau for careful reading of this manuscript.

References and notes

1 J. Reedijk, *Proc. Natl. Acad. Sci. U. S. A.*, 2003, **100**, 3611–3616.
2 E. Wong and C. M. Giandomenico, *Chem. Rev.*, 1999, **99**, 2451–2466.
3 J. Reedijk, *Chem. Rev.*, 1999, **99**, 2499–2510.
4 E. R. Jamieson and S. J. Lippard, *Chem. Rev.*, 1999, **99**, 2467–2498.
5 H. Zorbas and B. K. Keppler, *ChemBioChem*, 2005, **6**, 1157–1166.
6 D. Wang and S. J. Lippard, *Nat. Rev. Drug Discovery*, 2005, **4**, 307–320.
7 J. Reedijk, *Curr. Opin. Chem. Biol.*, 1999, **3**, 236–240.
8 M. A. Jakupec, M. Galaski and B. K. Keppler, *Rev. Physiol., Biochem., Pharmacol.*, 2003, **146**, 1–54.
9 C. X. Zhang and S. J. Lippard, *Curr. Opinion. Chem. Biol.*, 2003, **7**, 481–489.
10 E. Alessio, G. Mestroni, A. Bergamo and G. Sava, *Curr. Top. Med. Chem.*, 2004, **4**, 1525–1535.
11 E. Alessio, G. Mestroni, A. Bergamo and G. Sava, *Met. Ions Biol. Syst.*, 2004, **42**, 323–351.
12 (*a*) P. B. Arimondo and C. Hélène, *Curr. Med. Chem.: Anti-Cancer Agents*, 2001, **1**, 219–235; (*b*) M. D'Incalci and C. Sessa, *Expert Opin. Invest. Drugs*, 1997, **6**, 875–884.
13 (*a*) P. G. Baraldi, A. Bovero, F. Fruttarolo, D. Preti, M. A. Tabrizi, M. G. Pavani and R. Romagnoli, *Med. Res. Rev.*, 2004, **24**, 475–528; (*b*) B. S. Reddy, S. M. Sondhi and J. W. Lown, *Pharmacol. Ther.*, 1999, **84**, 1–111.
14 (*a*) A. Kamal, G. Ramesh, N. Laxman, P. Ramulu, O. Srinivas, K. Neelima, A. Kondapi, V. B. Sreenu and H. A. Nagarajaram, *J. Med. Chem.*, 2002, **45**, 4679–4688; (*b*) M. C. Alley, M. G. Hilligshead, C. M. Pacula-Cox, W. R. Waud, J. A. Hartley, P. W. Howard, S. J. Gregson, D. E. Thurston and E. A. Sausville, *Cancer Res.*, 2004, **64**, 6700–6706.
15 (*a*) H. A. Burris, V. C. Dieras, M. Tunca, R. H. Earhart, J. R. Eckardt, G. I. Rodriguez, D. S. Shaffer, S. M. Fields, E. Campbell, L. Schaaf, D. Kasunic and D. D. Von Hoff, *Anti-Cancer Drugs*, 1997, **8**, 588–596; (*b*) B. J. Foster, P. M. LoRusso, E. Poplin, M. Zalupski, M. Valdivieso, A. Wozniak, L. Flaherty, D. A. Kasunic, R. H. Earhart and L. H. Baker, *Invest. New Drugs*, 1996, **13**, 321–326.
16 J. V. Burda, M. Zeizinger and J. Leszczynski, *J. Comput. Chem.*, 2005, **26**, 907–914.
17 Y. Zhang, Z. Guo and X. Z. Yuo, *J. Am. Chem. Soc.*, 2001, **123**, 9378–9387.
18 (*a*) J. V. Burda, M. Zeizinger and J. Leszczynski, *J. Chem. Phys.*, 2004, **120**, 1253–1262; (*b*) M. Zeizinger, J. V. Burda and J. Leszczynski, *Phys. Chem. Chem. Phys.*, 2004, **6**, 3585–3590.
19 (*a*) A. Robertazzi and J. A. Platts, *J. Comput. Chem.*, 2004, **25**, 1060–1067; (*b*) A. Robertazzi and J. A. Platts, *J. Biol. Inorg. Chem.*, 2005, **10**, 854–866.
20 (*a*) L. A. S. Costa, W. R. Rocha, W. B. De Almeida and H. F. Dos Santos, *Chem. Phys. Lett.*, 2004, **387**, 182 and references therein; (*b*) L. A. S. Costa, W. R. Rocha, W. B. De Almeida and H. F. Dos Santos, *J. Inorg. Biochem.*, 2005, **99**, 575–583.
21 (*a*) P. Carloni, W. Andreoni, J. Hutter, A. Curioni, P. Giannozzi and M. Parrinello, *Chem. Phys. Lett.*, 1995, **234**, 50–56; (*b*) P. Carloni, M. Sprik and W. Andreoni, *J. Phys. Chem. B*, 2000, **104**, 823–835.
22 J. K. C. Lau and D. V. Deubel, *Chem. Eur. J.*, 2005, **11**, 2849–2855.
23 M. H. Baik, R. Friesner and S. J. Lippard, *J. Am. Chem. Soc.*, 2003, **125**, 14081–14092.
24 T. Zimmermann, M. Zeizinger and J. V. Burda, *J. Inorg. Biochem.*, 2005, **99**, 2184–2196.
25 J. Raber, C. B. Zhu and L. A. Eriksson, *J. Phys. Chem. B*, 2005, **109**, 11006–11015.
26 D. V. Deubel, *J. Am. Chem. Soc.*, 2004, **126**, 5999–6004.
27 J. Kozelka, *Met. Ions Biol. Syst.*, 1996, **33**, 1–28.
28 M. A. Elizondo-Riojas and J. Kozelka, *J. Mol. Biol.*, 2001, **314**, 1227–1243.
29 (*a*) A. Dorcier, P. J. Dyson, C. Gossens, U. Rothlisberger, R. Scopelliti and I. Tavernelli, *Organometallics*, 2005, **24**, 2114–2123; (*b*) C. Gossens, I. Tavernelli and U. Rothlisberger, *Chimia*, 2005, **59**, 81–84.
30 (*a*) P. Cimino, L. Gomez-Paloma and V. Barone, *J. Org. Chem.*, 2004, **69**, 7414–7442; (*b*) P. Cimino, R. Improta, G. Bifulco, R. Riccio, L. Gomez-Paloma and V. Barone, *J. Org. Chem.*, 2004, **69**, 2816–2824.
31 (*a*) M. Freccero and R. Gandolfi, *J. Org. Chem.*, 2005, **70**, 7098–7106; (*b*) M. Freccero and R. Gandolfi, *J. Org. Chem.*, 2004, **69**, 6202–6213.
32 P. Carloni, U. Rothlisberger and M. Parrinello, *Acc. Chem. Res.*, 2002, **35**, 455–464.
33 A. Magistrato and P. Carloni, 'Ab initio Molecular Dynamics Simulations of Biological Relevant Systems', in: *Handbook of Material Modeling*, ed. S. Yip, Springer, Netherlands, 2005, vol. 1, pp. 259–273.
34 P. Sherwood, in: *Modern Methods and Algorithms of Quantum Chemistry*, ed. J. Grotendorst, Forschungszentrum Juelich, 2000, NIC Series vol. 3, pp. 285–305.
35 M. Colombo, L. Guidoni, A. Laio, A. Magistrato, P. Maurer, S. Piana, U. Roehrig, K. Spiegel, M. Sulpizi, J. VandeVondele, M. Zumstain and U. Rothlisberger, *Chimia*, 2002, **56**, 13–19.
36 J. L. Gao and D. G. Truhlar, *Annu. Rev. Phys. Chem.*, 2002, **53**, 467–505.
37 R. A. Friesner and V. Guallar, *Annu. Rev. Phys. Chem.*, 2005, **56**, 389–427.
38 K. Spiegel, U. Rothlisberger and P. Carloni, *J. Phys. Chem. B*, 2004, **108**, 2699–2707.
39 A. Magistrato, P. Ruggerone, K. Spiegel, P. Carloni and J. Reedijk, *J. Phys. Chem. B*, 2006, **110**, 3604–3613.
40 A. V. Vargiu, P. Ruggerone, A. Magistrato and P. Carloni, *Nucleic Acid Res.*, submitted.
41 K. Spiegel, U. Rothlisberger and P. Carloni, *J. Phys. Chem. B*, 2006, **110**, 3647–3660.
42 A. Warshel and M. Levitt, *J. Mol. Biol.*, 1976, **2**, 227–249.
43 R. Car and M. Parrinello, *Phys. Rev. Lett.*, 1985, **55**, 2471–2474.
44 D. Marx and J. Hutter, in: *Modern Methods and Algorithms of Quantum Chemistry*, ed. J. Grotendorst, Forschungszentrum Juelich, 2000, NIC Series vol.1, pp. 301–449.
45 T. K. Woo, P. M. Margl, P. E. Bloch and T. Ziegler, *J. Phys. Chem.*, 1997, **101**, 7877–7880.
46 A. Laio, J. VandeVondele and U. Rothlisberger, *J. Chem. Phys.*, 2002, **116**, 6941–6947.
47 M. Eichinger, P. Tavan, J. Hutter and M. Parrinello, *J. Chem. Phys.*, 1999, **110**, 10452–10467.
48 J. Hutter, A. Alavi, T. Deutsch, P. Ballone, M. Bernasconi, P. Focher and S. Goedecker, *CPMD*, Max-Planck-Institut für Festkörperforschung (Stuttgart) and IBM Research, 1995–1999.
49 D. A. Case, D. A. Pearlman, J. W. Caldwell, T. E. Cheathman, III, W. S. Ross, C. L. Simmerling, T. A. Darden, K. M. Merz, R. V. Stanton, A. L. Cheng, J. J. Vincent, M. Crowley, V. Tsui, R. J. Radner, Y. Duan, J. Pitera, I. Massova, G. L. Seibel, U. C. Singh, P. K. Weiner, P. A. Kollman, *AMBER7*, University of California, San Francisco, CA, 2002.
50 D. A. Pearlman, D. A. Case, J. W. Caldwell, W. S. Ross, T. E. III Cheatham, S. DeBolt, D. Ferguson, G. L. Seibel and P. A. Kollman, *Comput. Phys. Commun.*, 1995, **91**, 1–41.
51 P. Hunenberger, *J. Chem. Phys.*, 2000, **113**, 10464–10467.
52 (*a*) M. Dal Peraro, L. I. Llarrull, U. Rothlisberger, A. J. Vila and P. Carloni, *J. Am. Chem. Soc.*, 2004, **126**, 12661–12668; (*b*) M. Cascella, C. Micheletti, U. Rothlisberger and P. Carloni, *J. Am. Chem. Soc.*, 2005, **127**, 3734–3742; (*c*) A. Magistrato, W. F. DeGrado, A. Laio, U. Rothlisberger, J. VandeVondele and M. L. Klein, *J. Phys. Chem. B*, 2003, **107**, 4182–4188.
53 P. M. Takahara, A. C. Rosenzweig, C. A. Frederick and S. J. Lippard, *Nature*, 1995, **377**, 649–652.
54 U. M. Ohndorf, M. A. Rould, Q. He, C. O. Pabo and S. J. Lippard, *Nature*, 1999, **399**, 708–712.
55 The structural models were initially equilibrated by classical MD simulations with the Amber force filed (W. D. Cornell, P. Cieplak, C. I. Bayly, I. R. Gould, K. M. Merz, D. M. Ferguson, D. C. Spellmeyer, T. Fox, J. W. Caldwell and P. A. Kollman, *J. Am. Chem. Soc.*, 1995, **117**, 5179–5197; T. E. III. Cheatham, P. Cieplak and P. A. Kollman, *J. Biomol. Struct. Dyn.*, 1999, **16**, 845–862). The TIP3P model was used for water (W. L. Joergensen, J. Chandrasekhar, J. D. Madura, R. W. Impey and M. L. Klein, *J. Chem. Phys.*, 1983, **79**, 926–935). Room-temperature simulations were achieved by coupling the systems to a Berendsen thermostat (H. J. C. Berendsen, J. P. M. Postma, W. F. van Gunsteren, A. DiNola and J. R. Haak, *J. Chem. Phys.*, 1984, **81**, 3684–3690).
56 In the QM/MM simulations we have adopted, the same computational setup as in ref. 66 was used for the MM part. For the QM region a plane waves (PW) basis set up to an energy cutoff of 70 Ry was used. Core/valence interactions were described using norm conserving pseudopotentials of the Martins–Troullier type (N. Trouiller and J. L. Martins, *Phys. Rev. B*, 1991, **43**, 1993–2006). Integration of the nonlocal parts of the pseudopotential was obtained by the Kleinman–Bylander scheme (L. Kleinman and D. M. Bylander, *Phys. Rev. Lett.*, 1982, **48**, 1425–1428) for all of the atoms except platinum, for which a Gauss–Hermite numerical integration scheme was used.

The gradient-corrected Becke exchange functional and the Lee–Yang–Parr correlation functional (BLYP) were used (A. D. Becke, *Phys. Rev. A*, 1998, **38**, 3098–3100; C. Lee, W. Yang and R. G. Parr, *Phys. Rev. B*, 1988, **37**, 785–789). Isolated system conditions were applied (R. N. Barnett and U. Landman, *Phys. Rev. B*, 1993, **48**, 2081–2097).
57 A. Gelasco and S. J. Lippard, *Biochemistry*, 1998, **37**, 9230–9239.
58 DNA structural parameters were calculated with the program *Curves* (S. Swaminathan, G. Ravishanker, D. L. Beveridge, R. Lavery, C. Etchebest and H. Sklenar, *Proteins: Struct., Funct., Genet.*, 1990, **8**, 179–193; R. Lavery and H. Sklenar, *J. Biomol. Struct. Dyn.*, 1989, **6**, 655–667).
59 S. Komeda, M. Lutz, A. L. Spek, M. Chikuma and J. Reedijk, *Inorg. Chem.*, 2000, **39**, 4230–4236.
60 S. Komeda, H. Ohishi, H. Yamane, M. Harikawa, K. Sakaguchi and M. Chikuma, *J. Chem. Soc., Dalton Trans.*, 1999, **17**, 2959–2962.
61 S. Telechtea, S. Komeda, J. M. Teuben, M. A. Elizondo-Riojas, J. Reedijk and J. Kozelka, 'A pyrazolate-bridged dinuclear platinum(II) complex induces only minor distortions upon DNA-binding', *Chem. Eur. J.*, 2006, **12**, 3741–3753.
62 (*a*) S. Komeda, S. Bombard, S. Perrier, J. Reedijk and J. Kozelka, *J. Inorg. Biochem.*, 2003, **96**, 357–366; (*b*) S. Komeda, H. Yamane, M. Chikuma and J. Reedijk, *Eur. J. Inorg. Chem.*, 2004, **24**, 4828–4835.
63 S. Komeda, M. Lutz, A. L. Spek, Y. Yamanaka, T. Sato, M. Chikuma and J. Reedijk, *J. Am. Chem. Soc.*, 2002, **124**, 4738–4746.
64 This angle refers to the angle between the normal vectors onto the mean plane of the base pair under consideration.
65 These structural changes are clearly limited by the time scale of our simulation (only a few ps). At the present we can perform an analysis of local parameters of the platinated moiety, while longer scale molecular dynamics simulations are required in order to have converged global parameters.
66 (*a*) F. Ercolessi and J. B. Adams, *Europhys. Lett.*, 1994, **26**, 583–588; (*b*) P. Maurer, 'First-principles characterization of radiopharmaceuticals and steps towards their rational design', diss. no. 15316, ETH, Zurich, ch. 5, pp. 121–150; (*c*) P. Maurer, A. Laio and U. Rothlisberger, 'On-the-fly parametrization of classical force field from QM/MM simulations', to be published.
67 K. Spiegel, A. Magistrato, P. Maurer, P. Ruggerone, U. Rothlisberger, P. Carloni, J. Reedijk and M. L. Klein, to be published.
68 M. L. Kopka, D. S. Goodsell, I. Baikalov, K. Grzeskowiak, D. Cascio and R. E. Dickerson, *Biochemistry*, 1994, **33**, 13593–13610.
69 C. Teijeiro, E. de la Red and D. Marin, *Electroanalysis*, 2000, **12**, 963–968.
70 (*a*) Boys orbitals (BO) are obtained by a unitary transformation of the delocalized Kohn–Sham orbitals, under the constraint to minimize the spread-function S:

$$S = \sum_{n=1}^{N} (\langle w_n | r^2 | w_n \rangle - \langle w_n | r | w_n \rangle^2)$$

where w_n refers to the transformed orbital. Boys centers (BCs) are obtained by the position of maximal density of each BO. The bond ionicity (BI) for a given bond X–Y is then calculated as the ratio

$$\frac{r_{\mathrm{X-BC}} \cdot \cos\theta}{r_{\mathrm{X-Y}}}$$

where $\cos\theta$ is the angle between $r_{\mathrm{X-BC}}$ and $r_{\mathrm{X-Y}}$. For more details, see: N. Marzari and D. Vanderbilt, *Phys. Rev. B*, 1997, **56**, 12847–12865; (*b*) F. Alber, G. Folkers and P. Carloni, *J. Phys. Chem. B*, 1999, **103**, 6121–6126.
71 P. S. Eis, J. A. Smith, J. M. Rydzewski, D. A. Case, D. L. Boger and W. J. Chazin, *J. Mol. Biol.*, 1997, **272**, 237–252.
72 C. H. Lin and D. J. Patel, *J. Mol. Biol.*, 1995, **248**, 162–179.
73 T. Yasuzawa, K. Muroi, M. Ichimura, I. Takahashi, T. Ogawa, K. Takahashi, H. Sano and Y. Saitoh, *Chem. Pharm. Bull.*, 1995, **43**, 378–391.
74 E. J. Small, R. Figlin, D. Petrylak, D. J. Vaughn, O. Sartor, I. Horak, R. Pincus, A. Kremer and C. Bowden, *Invest. New Drugs*, 2000, **18**, 193–197.
75 D. L. Boger and R. M. Garbaccio, *Bioorg. Med. Chem.*, 1997, **5**, 263–276.
76 D. L. Boger and R. M. Garbaccio, *Acc. Chem. Res.*, 1999, **32**, 1043–1052.
77 D. Sun, C. H. Lin and L. H. Hurley, *Biochemistry*, 1993, **32**, 4487–4495.
78 J. R. Schnell, R. R. Ketchem, D. L. Boger and W. J. Chazin, *J. Am. Chem. Soc.*, 1999, **121**, 5645–5652.
79 G. Lamm, L. Wong and G. R. Pack, *J. Am. Chem. Soc.*, 1996, **118**, 3325–3331.
80 M. A. Warpehoski and D. E. Harper, *J. Am. Chem. Soc.*, 1994, **116**, 7573–7580.
81 In the thermodynamic integration approach, a suitable reaction coordinate is chosen, which is varied by small increments until the transition state is reached. Here, we chose the distance between N3@Ade and C13@drug. The force at each step along the reaction coordinate is obtained by averaging over the trajectory, which typically spans 3–5 ps. At the transition state, the average force is 0. An estimate of the activation barrier is obtained by numerical integration of the constraint-force over the reaction coordinate: $\Delta F^{\#} = \Sigma \langle \mathrm{f}(r) \rangle \Delta r$ where $\langle \mathrm{f}(r) \rangle$ is the average force at step r, and Δr is the increment of the reaction coordinate. See: E. A. Carter, G. Ciccotti, J. T. Hynes and R. Kapral, *Chem. Phys. Lett.*, 1989, **156**, 472–477.
82 J. VandeVondele and U. Rothlisberger, *J. Phys. Chem. B*, 2002, **106**, 203–208.
83 M. Iannuzzi, A. Laio and M. Parrinello, *Phys. Rev. Lett.*, 2003, **90**, 2383302.
84 M. Cascella, L. Guidoni, U. Rothlisberger, A. Maritan and P. Carloni, *J. Phys. Chem. B*, 2002, **106**, 13027–13032.
85 M. Iannuzzi, A. Laio and M. Parrinello, *Phys. Rev. Lett.*, 2003, **90**, article no. 238302.
86 A. Stirling, M. Iannuzzi, A. Laio and M. Parrinello, *ChemPhysChem*, 2004, **5**, 1558–1568.